Comptes Rendus

Mécanique

Ala Eddin Chakroun, Ahmed Hammami, Ana De-Juan, Fakher Chaari, Alfonso Fernandez, Fernando Viadero and Mohamed Haddar

Modal energetic analysis and dynamic response of worm gear drives with a new developed dynamic model

Short paper / *Note*

Modal energetic analysis and dynamic response of worm gear drives with a new developed dynamic model

Ala Eddin Chakroun[a, b], **Ahmed Hammami**[a], **Ana De-Juan**[b],
Fakher Chaari∗, [a], **Alfonso Fernandez**[b], **Fernando Viadero**[b]
and Mohamed Haddar[a]

[a] Mechanics, Modelling and Production Laboratory, National School of Engineers Sfax, Tunisia

[b] Department of Structural and Mechanical Engineering, University of Cantabria, Spain

E-mails: Chakroun.ala.eddin@gmail.com (A. E. Chakroun),
ahmed.hammami2109@gmail.com (A. Hammami), ana.dejuan@unican.es
(A. De-Juan), fakher.chaari@gmail.com (F. Chaari), alfonso.fernandez@unican.es
(A. Fernandez), fernando.viadero@unican.es (F. Viadero),
mohamed.haddar@enis.rnu.tn (M. Haddar)

Abstract. In order to investigate the behaviour of worm drives, a new dynamic model, composed of two blocks, is established and used to extract numerical results. The tooth deflection of the worm drive, bearings, and wheels inertias are taken into consideration. Newmark solving method is applied to solve motion equations. The state of contact of teeth is what enables these signals to manifest themselves. Modal analysis is developed to investigate the different natural modes of the model. Furthermore, modal energetic analysis is used to understand the distribution of strain and kinetic energies. It is also applied to classify natural models into "teeth modes" and "bearing modes". These two modes constitute two different frequency bands. The dynamic coefficient is measured simultaneously with the gradual increase of the turning speed of the motor. This allows for the evaluation of the overload of the system.

∗ Corresponding author.

1. Introduction

Over time, many types of gears, from simple spur gears to complex hypoid gears, have been established. Worm drives, for example, are characterized by transmission axes that do not cross but can put into different angles.Magyar and Sauer [1] take into account most of the factors of power loss in order to investigate the average efficiency of transmission. They bring to the fore a tribological calculation method that is complex but reliable. Other studies claim that it is important to investigate other factors. The studies of Sharif *et al.* [2] and Sharif *et al.* [3] focus on the pattern and rate of wear. They use lubricant and predict the evolution of wear over time. Some studies were theoretical. Falah and Elkholy [4] used their original slicing method to determine the stiffness, load, and stress distribution. Chen and Tsay developed a mathematical model to generate the geometry of a unique type of worm gear [5]. Some studies tried to find a better geometrical characteristics of worm gears by creating new forms. In the study of Simon [6], a new type of cylindrical worm gear drive has been developed. The idea is having a worm gear with a double arc profile while the worm has a concave profile. This type of gear showed a favourable position of the instantaneous contact line, a higher load carrying capacity, and a lower power loss in the oil film compared with common worm drives.

Other researchers found it interesting to study the behaviour of worm drives made with plastic. In the study of Marshek and Chan [7], it was found that pitting and ridging are major wear types. Both were followed with microcracks. This conclusion is the result of investigating the sliding contact surface of the gear pair using a scanning electron microscope. In the studies of Hiltcher *et al.* [8], the generalized Kelvin model was used to compute the viscoelastic displacement of the worm gear made of polymer. The quasi-static load sharing was investigated. The result of this study is that load sharing, meshing stiffness, and loaded transmission error depends on the speed of the rotation of the gears. de Vaujany *et al.* [9] used the same model and found correct correlations between simulation and measurements. They showed that the revolution speed modifies the mean value of the transmission error while the amplitude stayed the same. They also found that temperature have a big influence on the shape and the amplitude of the transmission error signal.

Regarding the existing dynamic models show reliable results but with many limitations. Benabid and Mansouri [10] introduce an original eight-degrees-of-freedom model. They try not to overload the model and to keep it as simple as possible. This model does not take into consideration the behaviour of bearings and other inertias in the system. Chung and Shaw [11] used a model with a flywheel. They solved a dynamic equation of transmission to predict the dynamic behaviour of such model. No bearings have been added and the flywheel remains very specific to this model. Liu *et al.* [12] attempted to use the spur gear dynamic model proposed by Tamminana *et al.* [13] in order to predict the dynamic performance of a worm drive. Jiang *et al.* [14] used the computer aided design model and import it into the ADAMS dynamic model in order to investigate the dynamic response to friction of a spur gear couple. All these models do not consider the bearing behaviour, the geometry of the worm drive, or the state of the surface of contact of the teeth.

In this study, a new dynamic worm drive model is proposed, based on previous research on other types of gears. A single-stage spur gear model established by Chaari *et al.* [15]. Two-stage gear model proposed by Beyaoui *et al.* [16]. Farhat *et al.* [17] proposed a numerical model of a single-stage gear box operating under variable stationary regime. They studied the interaction between gear mesh and bearings excitation in case of variable speed and load. Hmida *et al.* [18] adopted the model of Chaari et al. with the addition of an elastic couple. Instead of the elastic couple, a clutch has been used by Walha *et al.* [19] in a helical gear model. Bevel gears were modelled by Driss *et al.* [20]. Planetary gears were modelled by various researchers such as
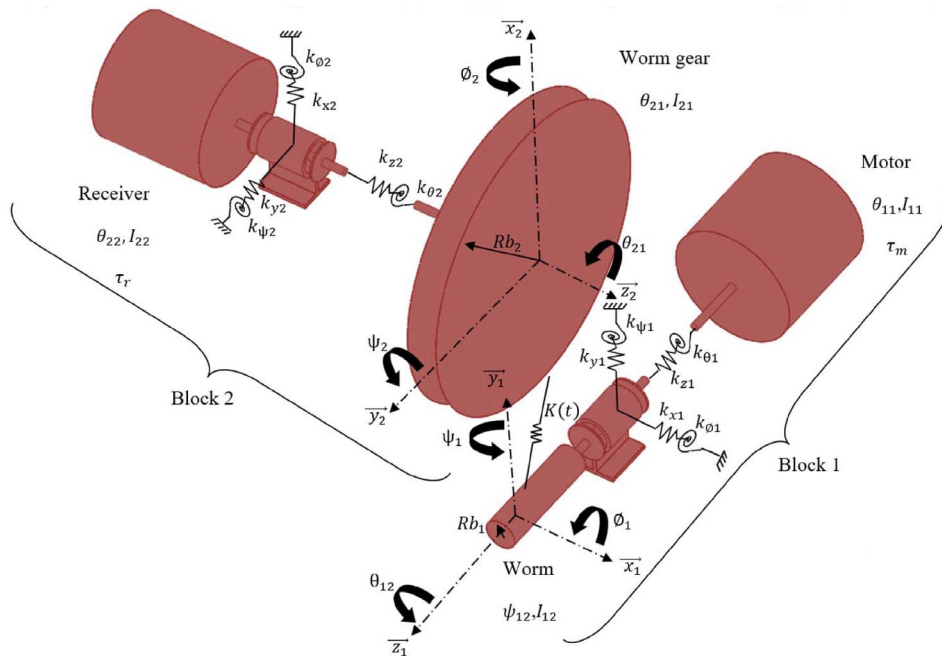
Figure 1. The dynamic model of the worm drive.

Hammami *et al.* [21], Bouslema *et al.* [22], and Feki *et al.* [23]. With the same approach, the new dynamic model is composed of two blocks and it has fourteen degrees of freedom. It takes into account the geometry of the worm drive, the bearings of the two blocks, and the inertias of gears, motor, and receiver. The equation of motion is obtained through Lagrange formalism after computing the deflection of contact of gear teeth. In this study, the gear mesh stiffness is modelled using an approximative approach. Advanced gear mesh stiffness with finite element modelling is used in the study of Fernandez Del Rincon *et al.* [24]. Newmark method is used to solve this equation. Through this model, modal analysis is carried out. This model also allows for the analyses of the modal energetic distributions. The analysis of the dynamic coefficient follows the study of the dynamic overload.

2. Dynamic model of worm gearbox

Figure 1 shows a kinematic chain of the worm reducer. The first block is composed of a motor, a bearing block, and a worm connected by a transmission shaft. The second block is composed of a receiver, a bearing block, and a worm gear that are connected also by a transmission shaft. Lagrange formalism is used to solve the equation of motion after taking into consideration the displacement in the line of action.

The motor and the receiver are deemed rigid bodies. The shafts are supposedly light weighted compared to other components. Their torsional and axial stiffness are $k_{\theta i}$ ($i = 1, 2$) and k_{zi} ($i = 1, 2$), respectively. Gear meshing and bearings are modelled using linear springs.

The translations of the two blocks are x_i, y_i, z_i ($i = 1, 2$) and the rotations are $\phi_i, \psi_i, \theta_{1i}, \theta_{2i}$ ($i = 1, 2$).

m_i is the weight of the worm when $i = 1$. m_i is the weight of the worm gear when $i = 2$. It is measured using the following equation

$$m_i = \pi b_i r_i^2 \rho_i \quad (i = 1, 2),\tag{1}$$

where b_i is the width of the worm gear when $i = 1$ and b_i is also the length of the worm when $i = 2$. ρ_i represents the material density. r_i is the pitch radius of the corresponding gear $(i = 1, 2)$.

I_{11} is the inertia of the motor. I_{12} is the inertia of the worm. I_{21} is the inertia of the worm gear. I_{22} is the inertia of the receiver.

2.1. *Calculation of transmission error*

The two points M_1 and M_2 belong to the active flank of the worm and the worm gear, respectively. Their relative displacement against a fixed benchmark $R(\vec{x}, \vec{y}, \vec{z})$ is calculated using the following:

$$\delta(l, t) = \overrightarrow{U_1^R(M_1)} \cdot \overrightarrow{n_1} + \overrightarrow{U_2^R(M_2)} \cdot \overrightarrow{n_2}\tag{2}$$

$\overrightarrow{U_i(M_i)}$: the displacement of M_i $(i = 1, 2)$,

$\overrightarrow{n_1}$ and $\overrightarrow{n_2}$ are the normal unitary outgoing vectors of M_i with $\overrightarrow{n_2} = -\overrightarrow{n_1}$.

In the action plan, l_i is the distance separating M_i from the middle of the line of action.

The gear pair is supposedly rigid. Both of the gears are rotating in the positive sense (counterclockwise). By taking into consideration the above mentioned conditions, it becomes possible to write the following:

$$\delta(l, t) = \left\{ \overrightarrow{U_1^R(O_1)} + \overrightarrow{\omega_1^R} \wedge \overrightarrow{O_1 M_1} \cdot \overrightarrow{n_1} - \overrightarrow{U_2^R(O_2)} - \overrightarrow{\omega_2^R} \wedge \overrightarrow{O_2 M_2} \cdot \overrightarrow{n_1} \right\}.\tag{3}$$

The displacement torsors of O_1 and O_2 are expressed against a fixed benchmark $R(\vec{x}, \vec{y}, \vec{z})$.

$$\delta\{\tau_1^R\} = \begin{cases} \overrightarrow{U_1^R(O_1)} = x_1 \vec{x} + y_1 \vec{y} + z_1 \vec{z} \\ \overrightarrow{\omega_1^R} = \varnothing_1 \vec{x} + \psi_1 \vec{y} + \theta_{12} \vec{z} \end{cases}\tag{4}$$

$$\delta\{\tau_2^R\} = \begin{cases} \overrightarrow{U_2^R(O_2)} = x_2 \vec{x} + y_2 \vec{y} + z_2 \vec{z} \\ \overrightarrow{\omega_2^R} = \varnothing_2 \vec{x} + \psi_2 \vec{y} + \theta_{21} \vec{z}. \end{cases}\tag{5}$$

The deflexion between the worm and the worm gear is calculated. Both are rotating in the positive sense (Figure 2).

The normal outgoing vector from the worm is expressed as

$$\overrightarrow{n_1} = \overrightarrow{Q_1 Q_2} \cos\beta + \sin\beta \overrightarrow{x_1}\tag{6}$$

$\overrightarrow{Q_1 Q_2}$ is the vector that represents the direction of movement

$$\overrightarrow{Q_1 Q_2} = -\sin(\gamma - \alpha)\overrightarrow{y_1} + \cos(\gamma - \alpha)\overrightarrow{z_1}\tag{7}$$

$\overrightarrow{O_1 M_1}$ positions M_1 in the worm using the following:

$$\overrightarrow{O_1 M_1} = \overrightarrow{O_1 Q_1} + \overrightarrow{Q_1 P_1} + \overrightarrow{P_1 M_1}\tag{8}$$

$$\overrightarrow{O_1 Q_1} = R_{b1}\overrightarrow{y_1} - Q_1 Q_2 \sin(\alpha - \gamma)\overrightarrow{z_1} \quad \text{with} \quad Q_1 Q_2 = \frac{R_{b1}}{\cos(\alpha - \gamma)}\tag{9}$$

R_{b1} is the base radius of the worm and R_{b2} is the base radius of the worm gear.

$$\overrightarrow{Q_1 P_1} = p_1 \overrightarrow{Q_1 Q_2}\tag{10}$$

$$\overrightarrow{P_1 M_1} = l_1 \cos\beta \overrightarrow{x_1} - l_1 \sin\beta \overrightarrow{Q_1 Q_2}\tag{11}$$

Figure 2. Modelling of the teeth contact of the gears.

$\overrightarrow{\omega_1}$ is the rotation vector in $(\overrightarrow{x_1}, \overrightarrow{y_1}, \overrightarrow{z_1})$. The translation of M_1 is expressed as follows:

$$\overrightarrow{U_1^R(M_1)} = \overrightarrow{U(O_1)} + \overrightarrow{\omega_1} \wedge \overrightarrow{O_1 M_1} \tag{12}$$

$$\overrightarrow{U_1^R(M_1)} = \begin{pmatrix} x_1 \\ y_1 \\ z_1 \end{pmatrix} + \begin{pmatrix} \varnothing_1 \\ \psi_1 \\ \theta_{12} \end{pmatrix} \wedge \begin{pmatrix} l_1 \cos\beta \\ Rb_1 + \sin(\gamma - \alpha)(l_1 \sin\beta - p_1) \\ -Rb_1 \tan(\alpha - \gamma) + (p_1 - l_1 \sin\beta)\cos(\gamma - \alpha) \end{pmatrix}. \tag{13}$$

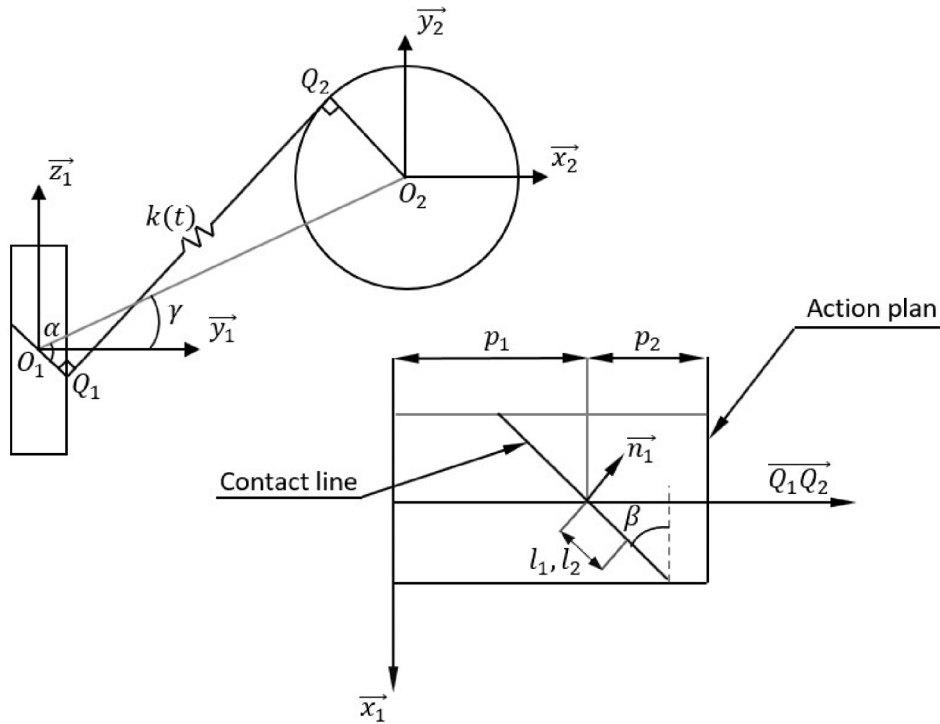On the other hand, M_2 of the worm gear is positioned by $\overrightarrow{O_2 M_2}$

$$\overrightarrow{O_2 M_2} = \overrightarrow{O_2 Q_2} + \overrightarrow{Q_2 P_2} + \overrightarrow{P_2 M_2} \tag{14}$$

$$\overrightarrow{O_2 Q_2} = Rb_2 \cos(\alpha - \gamma)\overrightarrow{x_2} - Rb_2 \sin(\alpha - \gamma)\overrightarrow{y_2} \tag{15}$$

$$\overrightarrow{Q_2 P_2} = -p_2 \overrightarrow{Q_1 Q_2} = p_2 \sin(\gamma - \alpha)\overrightarrow{x_2} - p_2 \cos(\gamma - \alpha)\overrightarrow{y_2} \tag{16}$$

$$\overrightarrow{P_2 M_2} = l_2 \cos\beta \overrightarrow{z_2} - l_2 \sin\beta \overrightarrow{Q_1 Q_2}. \tag{17}$$

The translation of M_2 in $(\overrightarrow{x_2}, \overrightarrow{y_2}, \overrightarrow{z_2})$ is

$$\overrightarrow{U_2^R(M_2)} = \overrightarrow{U(O_2)} + \overrightarrow{\omega_2} \wedge \overrightarrow{O_2 M_2} \tag{18}$$

$$\overrightarrow{U_2^R(M_2)} = \begin{pmatrix} x_2 \\ y_2 \\ z_2 \end{pmatrix} + \begin{pmatrix} \varnothing_2 \\ \psi_2 \\ \theta_{21} \end{pmatrix} \wedge \begin{pmatrix} -Rb_2 \cos(\alpha - \gamma) + \sin(\gamma - \alpha)(l_2 \sin\beta + p_2) \\ Rb_2 \sin(\alpha - \gamma) - (p_2 + l_2 \sin\beta)\cos(\gamma - \alpha) \\ l_2 \cos\beta \end{pmatrix}. \tag{19}$$

The deflexion $\delta(l, t)$ is

$$\begin{aligned} \delta(l, t) &= \overrightarrow{U_1^R(M_1)} \cdot \overrightarrow{n_1} + \overrightarrow{U_2^R(M_2)} \cdot \overrightarrow{n_2} \\ &= t_1(x_2 - y_1) + t_2(y_2 - z_1) + t_3(z_2 - x_1) + t_4\varnothing_1 + t_5\psi_1 + t_6\theta_{12} + t_7\varnothing_2 + t_8\psi_2 + t_9\theta_{21}. \end{aligned} \tag{20}$$

Table 1. Parameters of the deflexion

t_1	$\cos\beta\sin(\gamma-\alpha)$
t_2	$-\cos\beta\cos(\gamma-\alpha)$
t_3	$-\sin\beta$
t_4	$(-Rb_1\sin\beta\tan(\alpha-\gamma)+(p_1-l_1\sin\beta)\sin\beta\cos(\gamma-\alpha))-Rb_1\sin\beta-\sin(\gamma-\alpha)\sin\beta(p_1-l_1\sin\beta)$
t_5	$-Rb_1\tan(\alpha-\gamma)\cos\beta\sin(\gamma-\alpha)+\cos\beta\sin(\gamma-\alpha)\cos(\gamma-\alpha)(p_1-l_1\sin\beta)-l_1\cos^2\beta\sin(\gamma-\alpha)$
t_6	$Rb_1\cos\beta\cos(\gamma-\alpha)+\sin(\gamma-\alpha)(l_1\sin\beta+p_1)\cos\beta\cos(\gamma-\alpha)-l_1\cos^2\beta\cos(\gamma-\alpha)$
t_7	$-l_2\cos^2\beta\sin(\gamma-\alpha)+Rb_2\sin(\alpha-\gamma)\sin\beta-(p_2+l_2\sin\beta)\sin\beta\cos(\gamma-\alpha)$
t_8	$l_2\cos^2\beta\cos(\gamma-\alpha)-Rb_2\cos(\alpha-\gamma)\sin\beta+\sin(\gamma-\alpha)\sin\beta(p_2+l_2\sin\beta)$
t_9	$Rb_2\cos\beta-(p_2+l_2\sin\beta)\cos(\gamma-\alpha)\cos\beta(\cos(\gamma-\alpha)+\sin(\gamma-\alpha))$

The constants of the deflexion are presented in Table 1.

2.2. *The equation of motion*

The expression of the kinetic energy of the two blocks is in the following form

$$T = \tfrac{1}{2}m_1(\dot{x}_1^2+\dot{y}_1^2+\dot{z}_1^2)+\tfrac{1}{2}I_{11}\dot{\theta}_{11}^2+\tfrac{1}{2}I_{12}\dot{\theta}_{12}^2+\tfrac{1}{2}(I_{11x}+I_{12x})\dot{\phi}_1^2$$
$$+\tfrac{1}{2}(I_{11y}+I_{12y})\dot{\psi}_1^2\tfrac{1}{2}m_2(\dot{x}_2^2+\dot{y}_2^2+\dot{z}_2^2)+\tfrac{1}{2}I_{21}\dot{\theta}_{21}^2+\tfrac{1}{2}I_{22}\dot{\theta}_{22}^2$$
$$+\tfrac{1}{2}(I_{21x}+I_{22x})\dot{\phi}_2^2+\tfrac{1}{2}(I_{21y}+I_{22y})\dot{\psi}_2^2. \tag{21}$$

The strain energy of the two blocks is the following form

$$U = \tfrac{1}{2}k_{x1}x_1^2+\tfrac{1}{2}k_{y1}y_1^2+\tfrac{1}{2}k_{z1}z_1^2+\tfrac{1}{2}k_{\phi1}\phi_1^2+\tfrac{1}{2}k_{\psi1}\psi_1^2+\tfrac{1}{2}k_{\theta1}(\theta_{11}-\theta_{12})^2$$
$$+\tfrac{1}{2}k_{x2}x_2^2+\tfrac{1}{2}k_{y2}y_2^2+\tfrac{1}{2}k_{z2}z_2^2+\tfrac{1}{2}k_{\phi2}\phi_2^2+\tfrac{1}{2}k_{\psi2}\psi_2^2$$
$$+\tfrac{1}{2}k_{\theta2}(\theta_{21}-\theta_{22})^2+\tfrac{1}{2}k_m(t)\delta^2(t). \tag{22}$$

The work of the generalized external forces of the system is written in the following form

$$W = \tau_m\theta_{11}+\tau_r\theta_{22}. \tag{23}$$

The differential equation system of the movement reaction is put in a matrix form

$$M\{\ddot{q}\}+C\{\dot{q}\}+([K_A]+[K(t)])\{q\} = \{F_0\}. \tag{24}$$

With

$$\{q\} = \{x_1, y_1, z_1, x_2, y_2, z_2, \phi_1, \psi_1, \phi_2, \psi_2, \theta_{11}, \theta_{12}, \theta_{21}, \theta_{22}\} \tag{25}$$

$[M]$ is the mass matrix

$$[M] = \begin{bmatrix} M_L & 0 \\ 0 & M_A \end{bmatrix} \tag{26}$$

$[M_L]$ is a matrix composed of the following weight terms

$$[M_L] = \mathrm{diag}(m_1, m_1, m_1, m_2, m_2, m_2) \tag{27}$$

$[M_A]$ is a matrix composed of the following inertia terms

$$[M_A] = \mathrm{diag}(I_{11x}+I_{12x}, I_{11y}+I_{12y}, I_{21x}+I_{22x}, I_{21y}+I_{22y}, I_{11}, I_{12}, I_{21}, I_{22}). \tag{28}$$

The matrix of the average stiffness is written as follows:

$$[K_A] = \begin{bmatrix} K_p & 0 \\ 0 & K_\theta \end{bmatrix} \tag{29}$$

K_p is composed of the stiffness of the bearing blocks. It is in the following form

$$[K_p] = \mathrm{diag}(k_{x1}, k_{y1}, k_{z1}, k_{x2}, k_{y2}, k_{z2}) \tag{30}$$

$[K_\theta]$ is composed of $[K_{\theta i}]$ which is the tensional stiffness of the shaft. $[K_{\varnothing i}]$ and $[K_{\psi i}]$ are the stiffnesses of the bearings. $[K_\theta]$ is in the following form

$$[K_\theta] = \begin{bmatrix} k_{\varnothing 1} & 0 & 0 & 0 & 0 & 0 & 0 & 0 \\ 0 & k_{\psi 1} & 0 & 0 & 0 & 0 & 0 & 0 \\ 0 & 0 & k_{\varnothing 2} & 0 & 0 & 0 & 0 & 0 \\ 0 & 0 & 0 & k_{\psi 2} & 0 & 0 & 0 & 0 \\ 0 & 0 & 0 & 0 & k_{\theta 1} & -k_{\theta 1} & 0 & 0 \\ 0 & 0 & 0 & 0 & -k_{\theta 1} & k_{\theta 1} & 0 & 0 \\ 0 & 0 & 0 & 0 & 0 & 0 & k_{\theta 2} & -k_{\theta 2} \\ 0 & 0 & 0 & 0 & 0 & 0 & -k_{\theta 2} & k_{\theta 2} \end{bmatrix} \tag{31}$$

$[K(t)]$ is the matrix of the mesh stiffness. It is time-dependent (constants $t_{1\ldots9}$ are given in Table 1).

$$[K(t)] = \begin{bmatrix} K_{11}(t) & K_{12}(t) \\ K_{21}(t) & K_{22}(t) \end{bmatrix} \tag{32}$$

$$[K_{11}(t)] = k_m(t) \begin{bmatrix} t_3^2 & t_1 t_3 & t_2 t_3 & -t_1^2 & -t_1 t_2 & -t_1 t_3 \\ t_1 t_3 & t_1^2 & t_1 t_2 & -t_1 t_2 & -t_2^2 & -t_2 t_3 \\ t_2 t_3 & t_1 t_2 & t_2^2 & -t_1 t_3 & -t_2 t_3 & -t_3^2 \\ -t_1^2 & -t_1 t_2 & -t_1 t_3 & -t_1^2 & t_1 t_2 & t_1 t_3 \\ -t_1 t_2 & -t_2^2 & -t_2 t_3 & -t_1 t_2 & t_2^2 & t_2 t_3 \\ -t_1 t_3 & -t_2 t_3 & -t_3^2 & -t_1 t_3 & t_2 t_3 & t_3^2 \end{bmatrix} \tag{33}$$

$$[K_{12}(t)] = k_m(t) \begin{bmatrix} -t_1 t_4 & -t_1 t_5 & -t_1 t_6 & -t_1 t_7 & 0 & -t_1 t_8 & -t_1 t_9 & 0 \\ -t_2 t_4 & -t_2 t_5 & -t_2 t_6 & -t_2 t_7 & 0 & -t_2 t_8 & -t_2 t_9 & 0 \\ -t_3 t_4 & -t_3 t_5 & -t_3 t_6 & -t_3 t_7 & 0 & -t_3 t_8 & -t_3 t_9 & 0 \\ t_1 t_4 & t_1 t_5 & t_1 t_6 & t_1 t_7 & 0 & t_1 t_8 & t_1 t_9 & 0 \\ t_2 t_4 & t_2 t_5 & t_2 t_6 & t_2 t_7 & 0 & t_2 t_8 & t_2 t_9 & 0 \\ t_3 t_4 & t_3 t_5 & t_3 t_6 & t_3 t_7 & 0 & t_3 t_8 & t_3 t_9 & 0 \end{bmatrix} \tag{34}$$

$$[K_{21}(t)] = [K_{12}(t)]^T \tag{35}$$

$$[K_{22}(t)] = k_m(t) \begin{bmatrix} t_4^2 & t_4 t_5 & t_4 t_6 & t_4 t_7 & 0 & t_4 t_8 & t_4 t_9 & 0 \\ t_4 t_5 & t_5^2 & t_5 t_6 & t_5 t_7 & 0 & t_5 t_8 & t_5 t_9 & 0 \\ t_4 t_6 & t_5 t_6 & t_6^2 & t_6 t_7 & 0 & t_6 t_8 & t_6 t_9 & 0 \\ t_4 t_7 & t_5 t_7 & t_6 t_7 & t_7^2 & 0 & t_7 t_8 & t_7 t_9 & 0 \\ 0 & 0 & 0 & 0 & 0 & 0 & 0 & 0 \\ t_4 t_8 & t_5 t_8 & t_6 t_8 & t_7 t_8 & 0 & t_8^2 & t_8 t_9 & 0 \\ t_4 t_9 & t_5 t_9 & t_6 t_9 & t_7 t_8 & 0 & t_8 t_9 & t_9^2 & 0 \\ 0 & 0 & 0 & 0 & 0 & 0 & 0 & 0 \end{bmatrix}. \tag{36}$$

Figure 3 shows the geometrical parameters that the gear mesh stiffness $k_m(t)$ depends on. $L_{\max}$ and $L_{\min}$ are written as follows:

$$L_{\max} = (A \cdot B + A \cdot b + a \cdot B + c) \cdot l_1 \tag{37}$$

$$L_{\min} = (A \cdot B + A \cdot b + a \cdot B + (a + b - 1)) \cdot l_1 \quad \text{if } (a + b) > 1 \tag{38}$$

$$L_{\min} = (A \cdot B + A \cdot b + a \cdot B) \cdot l_1 \quad \text{if } (a + b) < 1. \tag{39}$$

A and B are integers. a and b are decimal functions and $c = a$ if $a < b$ and $c = b$ if $a \geq b$. $[C]$ is the damping matrix. It is applied following Rayleigh form

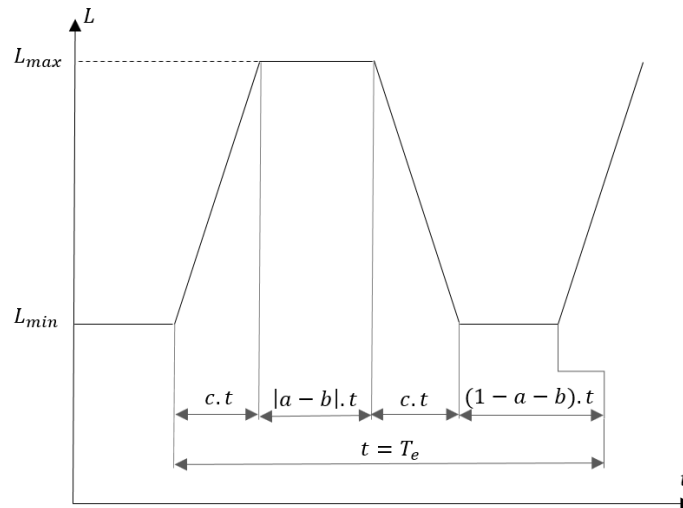$$[C] = \mu[K] + \lambda[M] \tag{40}$$

μ and λ are constants of proportionality.

The vector $\{F_0\}$ of the external static force is

$$\{F_0\} = \{0, 0, 0, 0, 0, 0, 0, 0, 0, 0, \tau_m, 0, 0, \tau_r\}^T. \tag{41}$$

Figure 3. Evolution of the length of the line of action.

Table 2. Characteristics of the worm drive

|	Worm	Worm gear
Number of teeth		50
Number of starts	1	
Gear material	Steel (S45C)	Bronze (CAC702)
Weight of the blocks (kg)	3.24	2.27
Rotation speed (rpm)	1500	30
Stiffnesses of the bearings (N/m)	$k_{x1} = k_{y1} = k_{x2} = k_{y2} = 10^8$	
Stiffnesses of the shafts (N/m)	$k_{z1} = k_{z2} = 2.1 \times 10^5$	
Torsional stiffnesses of the bearings (N·rd/m)	$k_{\phi1} = k_{\psi1} = k_{\phi2} = k_{\psi2} = 4 \times 10^7$	
Torsional stiffness of the shaft (N·rd/m)	$k_{\theta1} = k_{\theta2} = 8.4 \times 10^4$	
Modulus (m)	1×10^{-3}	
Normal pressure angle α_n	20°	
Lead angle γ	3.58°	
Parameters of the evolution of the line of action	$A = 3, B = 1, c = a = 0.7, b = 0.014$	
Parameters of the damping matrix	$\mu = 10^{-5}, \lambda = 0.05$ [25]	

3. Numerical results

The modal analysis of worm gearbox is carried out and its dynamic behaviour is studied. Parameters of the said gearbox are presented in Table 2.

3.1. *Modal analysis of the worm gear*

In this subsection, natural frequencies and modes are identified and the distribution of the modal strain and kinetic energies are analysed.

3.1.1. *Natural frequencies and natural modes*

Natural frequencies are identified in Figure 4 that presents frequency response function (FRF) of some degrees of freedoms (DOF). Said DOF are $x_2, y_2, \psi_2,$ and θ_{22}. The choice of said DOF was
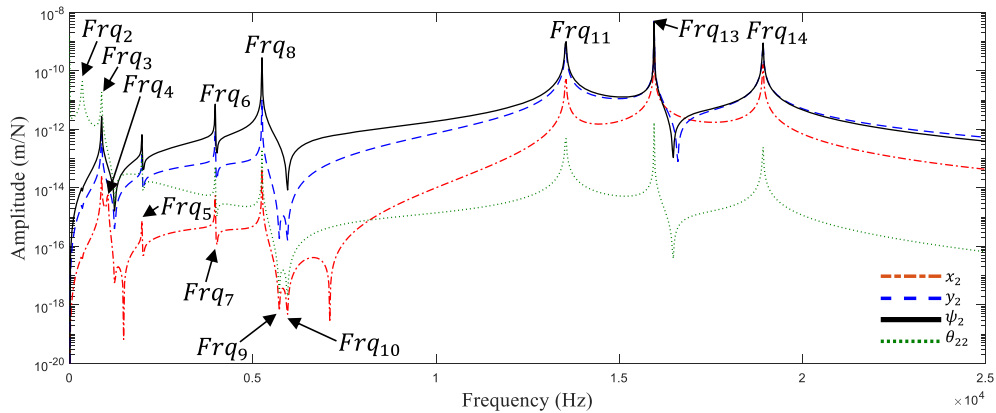
Figure 4. Frequency response function (FRF) of x_2, y_2, ψ_2, and θ_{22}.
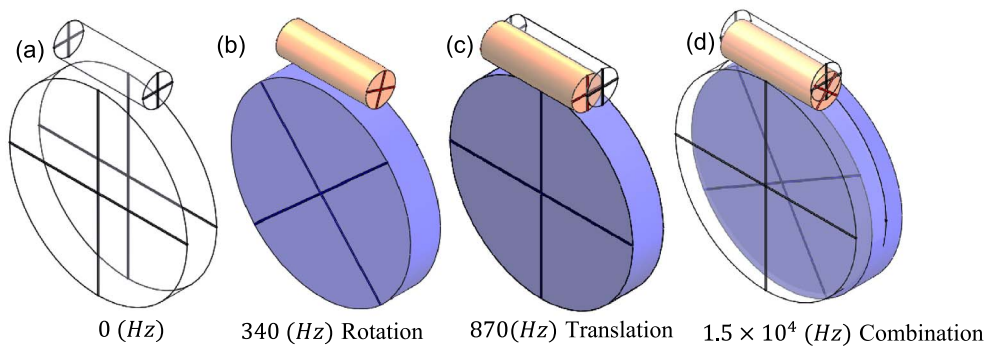
Figure 5. Examples of different mode shapes.

Table 3. Natural frequencies of the model

Frequency (Hz)	Natural mode	Frequency (Hz)	Natural mode
$Frq_1 = 0$	Rotation	$Frq_8 = 5251$	Rotation
$Frq_2 = 340$	Rotation	$Frq_9 = 5717$	Rotation
$Frq_3 = 870$	Translation	$Frq_{10} = 5863$	Combined
$Frq_4 = 1040$	Translation	$Frq_{11} = 1.35 \times 10^4$	Combined
$Frq_5 = 1980$	Rotation	$Frq_{12} = 1.5 \times 10^4$	Combined
$Frq_6 = 3972$	Rotation	$Frq_{13} = 1.6 \times 10^4$	Combined
$Frq_7 = 4010$	Rotation	$Frq_{14} = 1.89 \times 10^4$	Combined

based on the clarity of the figure. Other DOF have more or less the same shape with different amplitudes. The exceptions were in x_1, y_2, and z_1 that showed the minimum appearance of peaks specially in low natural frequencies.

This figure shows all the natural frequencies except Frq_1 (because $Frq_1 = 0$). All natural frequencies and their natural mode types are summarized in Table 3.

There are three types of natural modes: Translation, rotation, or a combination between both. Figure 5a is the rigid body mode. Figures 5b, c and d correspond respectively to a rotation, translation, and combined natural modes.

Table 4. Index j

j	1	2	3	4	5	6	7	8	9	10	11	12	13	14
DOF	x_1	y_1	z_1	x_2	y_2	z_2	$\emptyset_1$	ψ_1	$\emptyset_2$	ψ_2	θ_{11}	θ_{12}	θ_{21}	θ_{22}

Table 5. Index k

k	1	2	3	4	5	6	7	8	9	10	11	12
Stiffness	k_{x_1}	k_{y_1}	k_{z_1}	k_{x_2}	k_{y_2}	k_{z_2}	$k_{\emptyset_1}$	k_{ψ_1}	$k_{\emptyset_2}$	k_{ψ_2}	k_{θ_1}	k_{θ_2}

3.1.2. *Modal energetic analysis*

The modal strain energy and the modal kinetic energy for the mean value of mesh stiffness is written as the following expressions [26]. The total modal strain energy can be written as the sum of the strain energies of rotation and translation from each component. The total kinetic energy can also be written as the sum of the kinetic energies of rotation and translation from each component of the system

$$T_\emptyset = \frac{1}{2}\emptyset_k^t \tilde{K} \emptyset_k = \sum_{k=1}^{12} T_{\emptyset k} + T_{\emptyset w} \tag{42}$$

$$U_\emptyset = \frac{1}{2} w_j^2 \emptyset_j^t M \emptyset_j = \sum_{j=1}^{14} U_{\emptyset j}, \tag{43}$$

where j is the index of the corresponding DOF and k is the index of the corresponding stiffness. j and k are detailed in the following tables (Tables 4 and 5). $T_{\emptyset w}$ is the strain energy of the worm–worm gear meshing.

According to this modal energetic study, natural frequencies can be classified into two frequency bands: a band called "teeth modes" and a band called "bearing modes".

Teeth modes are characterized by a dominant modal strain energy located in the gear meshing and a dominant modal movement located in the worm or in the worm gear. While, bearing mode is characterized by a dominant modal strain energy located in the bearings. Figure 6 shows the distribution of the modal strain energies.

The X-axis of Figure 6 is detailed in Table 6. Figure 6 also shows that the bearing modes are located in a frequency band that starts in Frq_6 and ends in Frq_9. The dominant strain energies present the torsional stiffness of the bearings about X and Y direction. In all the other frequencies, the dominant strain energy represents gear meshing. In the later frequencies, the modes are called teeth modes. Unlike all the other frequencies of the teeth mode, the strain energies of Frq_2 and Frq_5 are not dominant in the gear meshing. In Frq_2, the dominant strain energy is divided between the torsional stiffness of the shaft of the second block about Z direction and gear meshing. In Frq_5, the strain energy is dominant in the torsional stiffness of the shaft of the first block about Z direction.

The X-axis of Figure 7 is detailed in Table 7. The first block rotates following Z and translates following X or Y. These motions do not have a dominant kinetic energy in any natural frequency. While each of the other 11 motions dominate in one or two natural frequencies each.

Table 8 summarizes the dominant modal movement and the dominant strain energy in low-frequency modes.

3.2. *Dynamic behaviour of worm gearbox*

In order to contribute to the study of the dynamic behaviour of worm gearbox, the dynamic response of said gearbox under ideal conditions is observed, and the evolution of its dynamic coefficient is evaluated.
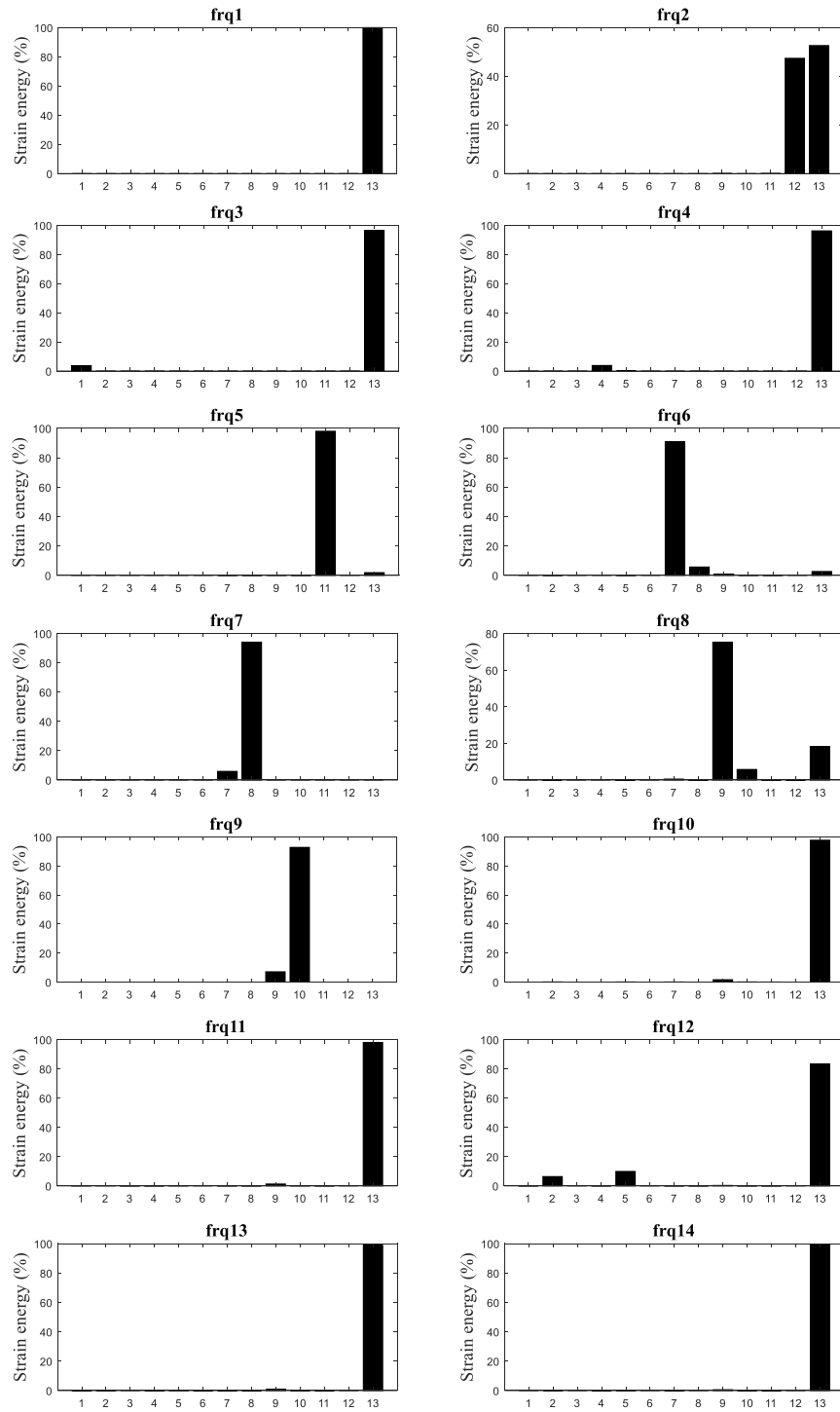
Figure 6. The distribution of strain energy.
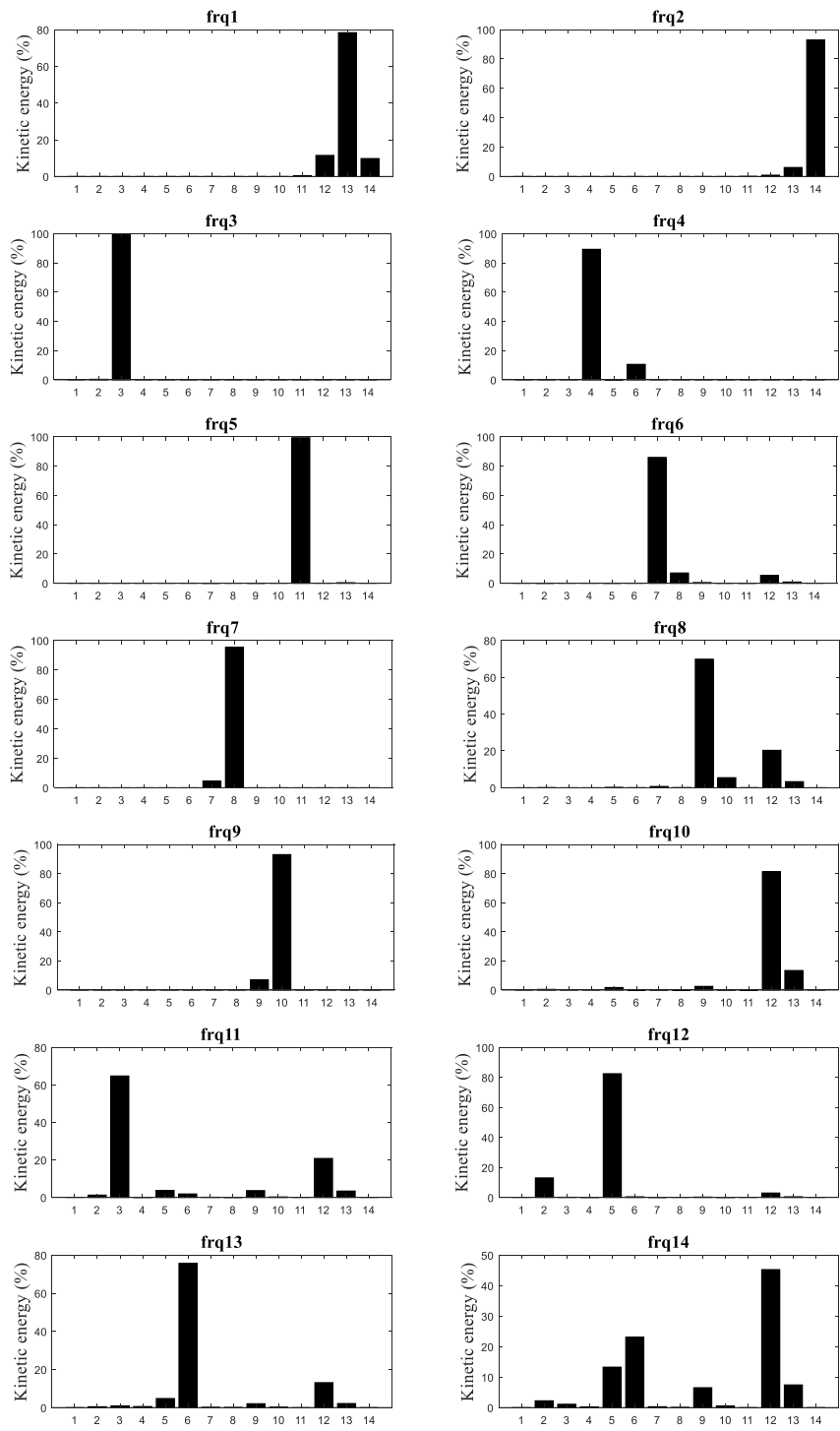
Figure 7. Kinetic energy distribution.

Table 6. X-axis of the strain energy distribution

1	Translational stiffness of the bearing of the first block in X	8	Translational stiffness of the bearing of the first block about Y
2	Translational stiffness of the bearing of the first block in Y	9	Torsional stiffness of the bearing of the second block about X direction
3	Translational stiffness of the shaft of the first block in Z	10	Torsional stiffness of the bearing of the second block about Y
4	Translational stiffness of the bearing of the second block in X	11	Torsional stiffness of the shaft of the first block about Z
5	Translational stiffness of the bearing of the second block in Y	12	Torsional stiffness of the shaft of the second block about Z
6	Translational stiffness of the shaft of the second block in Z	13	Gear meshing
7	Torsional stiffness of the bearing of the first block about X		

Table 7. X-axis of the kinetic energy distribution

1	Translation of the first block following X	8	Rotation of the first block following Y
2	Translation of the first block following Y	9	Rotation of the first block following X
3	Translation of the first block following Z	10	Rotation of the first block following Y
4	Translation of the second block following X	11	Rotation of the motor
5	Translation of the second block following Y	12	Rotation of the worm
6	Translation of the second block following Z	13	Rotation of the worm gear
7	Rotation of the first block following X	14	Rotation of the receiver

3.2.1. *Dynamic response of worm gearbox*

Figure 8 presents the gear mesh stiffness of the worm drive.

Solving the movement equation by using Newmark method provides the following results. Figure 9 shows the acceleration of the worm gear couple against a time frame.

The spectrum of the acceleration of the worm is presented in Figure 10. The first peak is the mesh frequency of the worm gear ($f_m = 25$ Hz). The following frequencies are its multiples. When the harmonic of the mesh frequency coincides with the natural frequency, disturbances occur in the spectrum. The first two disturbances coincide with the first observable natural frequencies Frq_2 and Frq_3.

### 3.2.2. *Dynamic overload*

In the study of [27], it is mentioned that, in a modal analysis, the parametric instability occur when harmonics of the mesh frequency are close to particular combinations of the natural frequencies. The instability appears when the following expressions are resulted

$$l f_m \approx Frq_a + Frq_b. \tag{44}$$

It is to say

$$f_m \approx \frac{Frq_a + Frq_b}{l} \tag{45}$$

for a and b are the index of a corresponding natural frequency and l is an integer. When $l = 1$ and $a = b$, it is called primary instability, when $l = 2$ and $a = b$, it is called secondary instability, and when $l = 1$ and $a \neq b$ it is called combination instability. Higher order instabilities can be found which is the case in this study. It is then important to do a load sweep on the mechanism
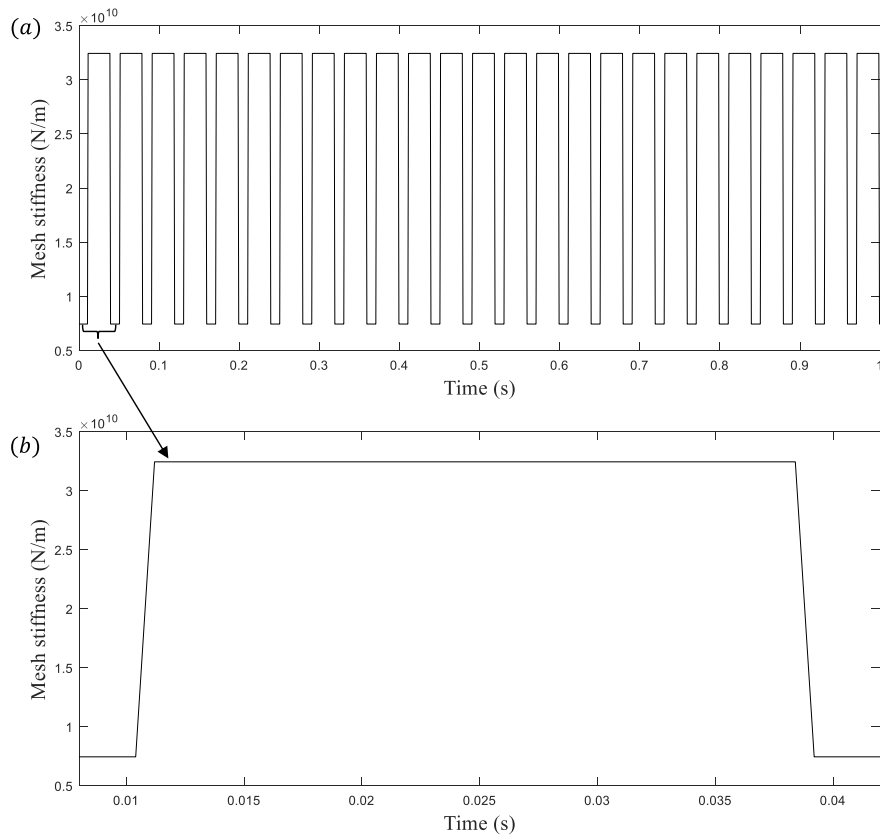
Figure 8. (a) Multiple and (b) single gear mesh stiffness against a time frame.
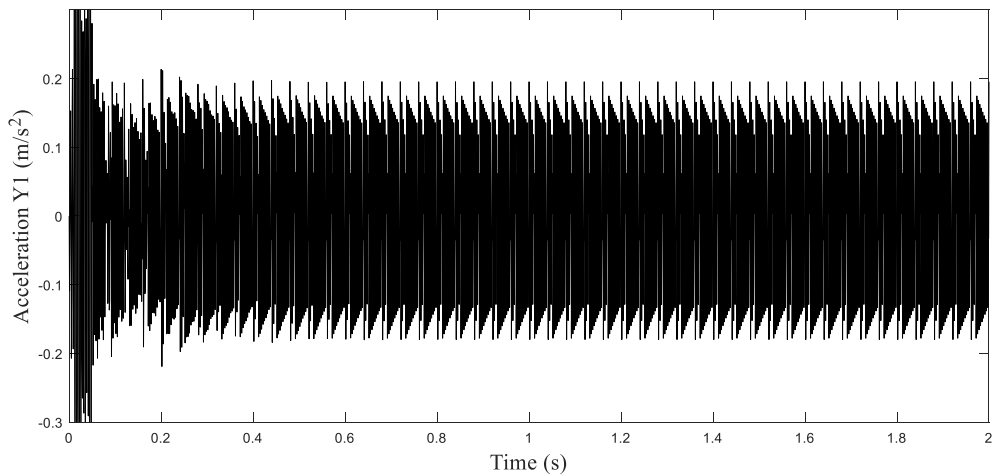
Figure 9. The time-dependent acceleration of the worm.

and extract the dynamic coefficient of loaded gear teeth. This allows for the identification of the critical areas of the system where overloaded gear teeth are found. The dynamic coefficient C_d is calculated using (46). F_D is the dynamic load that can be calculated using (47).
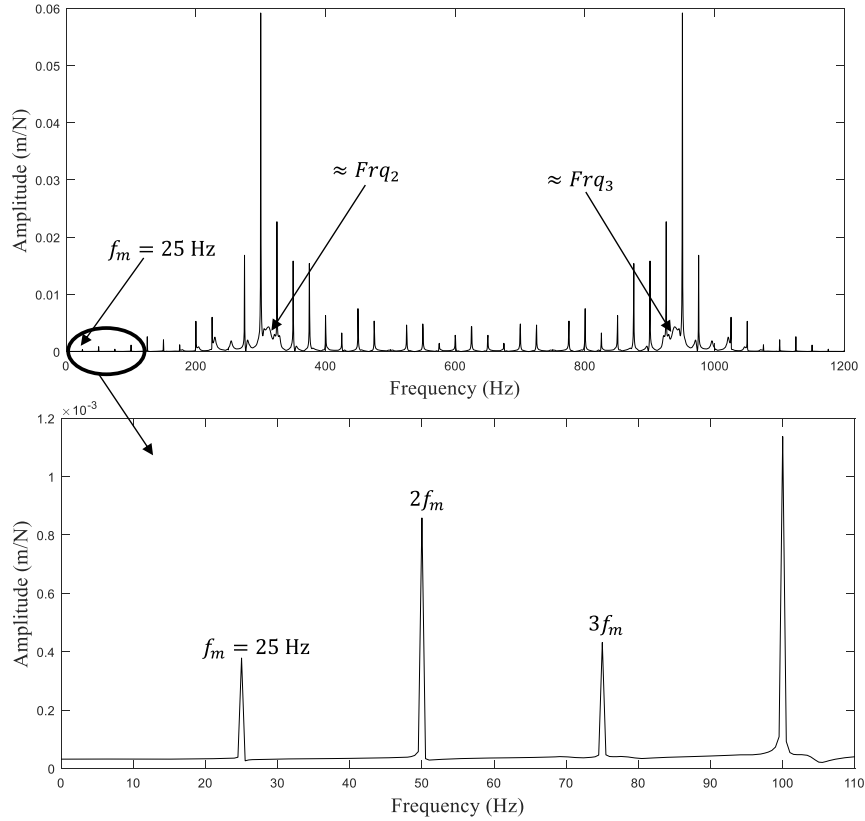
Figure 10. Spectrum the acceleration of the worm.

$$C_d = \frac{F_D}{F} \qquad (46)$$

$$F_D = F + F_{d\mathrm{RMS}} \qquad (47)$$

$$F_d(t) = K_m(t) * \delta(t). \qquad (48)$$

F is the static load applied by the receiver. It is considered that it is equal to nominal load that can be delivered by the motor. F_d is calculated using (48). It is the over load created by the dynamic components. $F_{d\mathrm{RMS}}$ is the RMS value of F_d. RMS stands for root mean square.

The dynamic coefficient is the result of a series of simulations in a frequency range that varies from 0 to 130 Hz. In this frequency band, the variation of the loads in the bearings is observed.
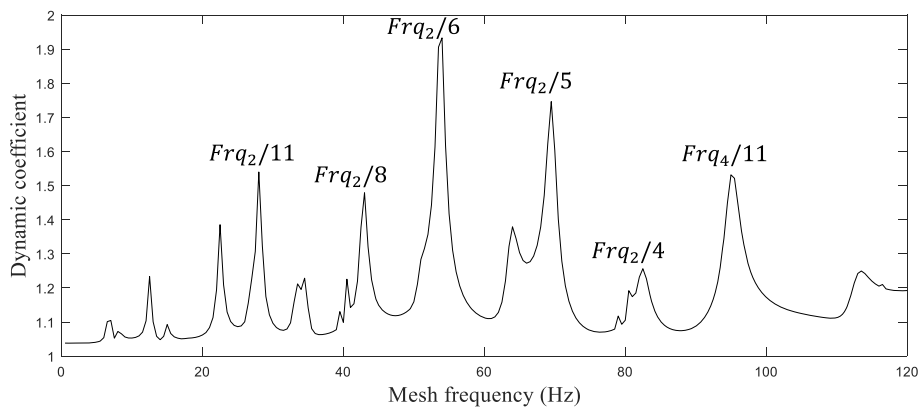
The evolution of the dynamic coefficient is presented in Figure 11. It is clear that there is an increase in the dynamic coefficient in certain mesh frequencies. Since this dynamic coefficient is the ratio of the dynamic load divided by the static load and thus results in the teeth dynamic overload. This can be explained by resonance of the mesh frequency with the harmonic of a natural frequency.

The dynamic coefficient is significant for $Frq_2/6$ and $Frq_2/5$ (deduced from (45)) as shown in Figure 11. The later frequencies correspond to 2690 rpm and 3475 rpm, respectively. These speeds cause the overload to become critical. The manufacturer must take into consideration these cases in order to avoid having the system functioning in critical conditions. For the other frequencies presented in Figure 11 ($Frq_2/11$, $Frq_2/8$, $Frq_2/4$, $Frq_4/11$), the increase in the dynamic coefficient is not too high, but it is better to not to overlook them. Overall, Frq_2 seems to

Table 8. Dominant motion and dominant strain energy in low frequencies

Frequency	Dominant modal movement	Dominant strain energy
Frq_1	Rotation of the worm gear	Gear meshing
Frq_2	Rotation of the receiver	Gear meshing
Frq_3	Translation of the shaft of the first block in Z direction	Gear meshing
Frq_4	Translation of the second block following X	Gear meshing
Frq_5	Translation of the second block following X	Torsional stiffness of the shaft of the first block following Z
Frq_6	Rotation of the first block following X	Torsional stiffness of the bearing of the first block following X
Frq_7	Rotation of the first block following Y	Torsional stiffness of the bearing of the first block following X
Frq_8	Rotation of the second block following X	Torsional stiffness of the bearing of the first block following Y
Frq_9	Rotation of the second block following Y	Torsional stiffness of the bearing of the first block following Y
Frq_{10}	Rotation of the worm Translation of the second block following Z	Gear meshing
Frq_{11}	Rotation of the worm Translation of the second block following Y	Gear meshing
Frq_{12}	Rotation of the worm Translation of the second block following Y	Gear meshing
Frq_{13}	Rotation of the worm Translation of the second block following Z	Gear meshing
Frq_{14}	Rotation of the worm Translation of the second block following Z	Gear meshing

Figure 11. Evolution of the dynamic coefficient.

be dominant for most of the overloads that appeared in the system. For this frequency, the strain energy was divided between the gear meshing and the torsional stiffness of the shaft of the first block about Z (Figure 6), which is a particular case. We call back that the normal case is having the dominant strain energy in the bearings for bearing modes and in gear meshing in teeth modes.

So, in order to avoid having problems in the system, this particular natural frequency must be taken into consideration.

4. Conclusion

A new dynamic worm gear model is proposed. This model takes into consideration the geometry and the contact conditions of the worm drive, bearings behaviour, and inertias. Modal analysis of worm gearbox is achieved using this model. Natural frequencies are identified through FRF. Natural modes are classified into rotational, translational, and combined modes. They are also classified according to their modal energetic distributions: (i) "teeth mode" is characterized by the dominant strain energy in the contact of the teeth of the worm gear and the dominant movement of gears and (ii) "bearing mode" is characterized by the dominant strain energy in the bearings.

   The proposed model of the worm gear also allows for the study of the dynamic of this gearbox. This gearbox is running under ideal conditions. It depends on the state of contact of the teeth. The spectrum of the dynamic coefficient shows several peaks at some gear mesh frequencies. In addition, the dynamic coefficient evolution allows to conclude that the dynamic load increases when a gear mesh frequency coincides with certain natural frequency or some other frequencies that divides natural frequencies.

Nomenclature

$k_{\theta i}$	The torsional stiffness	R_b	The base radius of the worm gear
k_{zi}	The axial stiffness	U	Strain energy of the model
k_{xi}, k_{yi}	The radial stiffness	W	The work of the system
x_i, y_i, z_i	The translations of the ith block	τ_m	The torque of the motor
$\varnothing_i, \psi_i \theta_{1i}, \theta_{2i}$	The rotations of the ith block	τ_r	The torque of the receiver
m_i	The weight of the ith block	M	The mass matrix
b_i	The width of the worm gear when $i = 1$ and the length of the worm when $i = 2$	C	The damping matrix
r_i	The radius of the ith gear	K_A	The average stiffness matrix
ρ_i	The density of the ith gear	$K(t)$	The mesh stiffness matrix
I_{11}	The inertia of the motor	μ, λ	Constants of proportionality of the damping matrix
I_{12}	The inertia of the worm	F_0	The vector of external static forces
I_{21}	The inertia of the worm gear	$T_\varnothing$	The modal kinetic energy
I_{22}	The inertia of the receiver	$U_\varnothing$	The modal strain energy
δ	The deflexion between the worm and the worm gear	w_i	The angular frequency of the ith block
M_i	The point belonging to the active flank of the ith gear	C_d	The dynamic coefficient
$\overrightarrow{U_i(M_i)}$	The displacement of M_i	F	The static load
$\overrightarrow{n_i}$	The normal unitary outgoing vectors of M_i	F_D	The dynamic force
l_i	The distance separating M_i from the middle of the line of action	F_d	The overload created by the dynamic component
T	Kinetic energy of the model	$F_{d\text{RMS}}$	The root mean square value of F_d
R_{b1}	The base radius of the worm		

References

[1] B. Magyar, B. Sauer, "Calculation of the efficiency of worm gear drives", in *International Gear Conference 2014, Lyon*, Woodhead Publishing Limited, 2014.

[2] K. J. Sharif, H. P. Evans, R. W. Snidle, D. Barnett, I. M. Egorov, "Effect of elastohydrodynamic film thickness on a wear model for worm gears", *Proc. Inst. Mech. Eng. Part J J. Eng. Tribol.* **220** (2006), no. 3, p. 295-306.

[3] K. J. Sharif, H. P. Evans, R. W. Snidle, "Prediction of the wear pattern in worm gears", *Wear* **261** (2006), no. 5–6, p. 666-673.

[4] A. H. Falah, A. H. Elkholy, "Load and stress analysis of cylindrical worm gearing using tooth slicing method", *Trans. Can. Soc. Mech. Eng.* **30** (2006), no. 1, p. 97-111.

[5] W. L. Chen, C. B. Tsay, "Mathematical model and tooth surfaces of recess action worm gears with double-depth teeth", *Mech. Mach. Theory* **46** (2011), no. 12, p. 1840-1853.

[6] V. Simon, "Displacements in worm gears with grouns concave worm profile", *Mech. Mach. Theory* **31** (1996), no. 8, p. 1131-1140.

[7] K. M. Marshek, P. K. C. Chan, "Wear damage to plastic worms and gears", *Wear* **44** (1977), no. 2, p. 405-409.

[8] Y. Hiltcher, M. Guingand, J.-P. de Vaujany, "Load sharing of worm gear with a plastic wheel", *J. Mech. Des.* **129** (2006), no. 1, p. 23-30.

[9] J.-P. de Vaujany, M. Guingand, D. Remond, "Numerical and experimental study of the loaded transmission error of a worm gear with a plastic wheel", *J. Mech. Des.* **130** (2008), no. 6, article no. 062602.

[10] Y. Benabid, S. Mansouri, "Dynamics study and diagnostics with vibration analysis from worm gear manufactured by reverse engineering techniques", *J. Vibroeng.* **18** (2016), no. 7, p. 4458-4471.

[11] M. Y. Chung, D. Shaw, "Parametric study of dynamics of worm and worm-gear set under suddenly applied rotating angle", *J. Sound Vib.* **304** (2007), no. 1–2, p. 246-262.

[12] Z. Y. Liu, C. C. Huang, Y. H. Hao, C. C. Lin, "The mesh property of the steel involute cylindrical worm with a plastic involute helical gear", *J. Mech.* **30** (2014), no. 2, p. 185-192.

[13] V. K. Tamminana, A. Kahraman, S. Vijayakar, "A study of the relationship between the dynamic factors and the dynamic transmission error of spur gear pairs", *J. Mech. Des.* **129** (2007), no. 1, p. 75-84.

[14] L. Jiang, Z. Deng, F. Gu, A. D. Ball, X. Li, "Effect of friction coefficients on the dynamic response of gear systems", *Front. Mech. Eng.* **12** (2017), no. 3, p. 397-405.

[15] F. Chaari, W. Baccar, M. S. Abbes, M. Haddar, "Effect of spalling or tooth breakage on gearmesh stiffness and dynamic response of a one-stage spur gear transmission", *Eur. J. Mech. A/Solids* **27** (2008), no. 4, p. 691-705.

[16] M. Beyaoui, M. Tounsi, K. Abboudi, N. Feki, L. Walha, M. Haddar, "Dynamic behaviour of a wind turbine gear system with uncertainties", *C. R. Mec.* **344** (2016), no. 6, p. 375-387.

[17] M. H. Farhat, T. Hentati, X. Chiementin, F. Bolaers, F. Chaari, M. Haddar, "Numerical model of a single stage gearbox under variable regime", *Mech. Based Des. Struct. Mach.* **50** (2020), https://doi.org/10.1080/15397734.2020.1863226.

[18] A. Hmida, A. Hammami, M. Taoufik Khabou, F. Chaari, M. Haddar, "Effect of elastic coupling on the modal characteristics of spur gearbox system", *Appl. Acoust.* **144** (2019), p. 71-84.

[19] L. Walha, Y. Driss, M. T. Khabou, T. Fakhfakh, M. Haddar, "Effects of eccentricity defect on the nonlinear dynamic behavior of the mechanism clutch-helical two stage gear", *Mech. Mach. Theory* **46** (2011), no. 7, p. 986-997.

[20] D. Yassine, H. Ahmed, W. Lassaad, H. Mohamed, "Effects of gear mesh fluctuation and defaults on the dynamic behavior of two-stage straight bevel system", *Mech. Mach. Theory* **82** (2014), p. 71-86.

[21] A. Hammami, A. F. Del Rincon, F. Chaari, F. V. Rueda, M. Haddar, "Dynamic behaviour of back to back planetary gear in run up and run down transient regimes", *J. Mech.* **31** (2015), no. 4, p. 481-491.

[22] M. Bouslema, A. Frikha, M. Abdennadhar, T. Fakhfakh, R. Nasri, M. Haddar, "Effects of modal truncation and condensation methods on the frequency response function of a stage reducer connected by rigid coupling to a planetary gear system", *C. R. Mec.* **345** (2017), no. 12, p. 807-823.

[23] N. Feki, M. Karray, M. T. Khabou, F. Chaari, M. Haddar, "Frequency analysis of a two-stage planetary gearbox using two different methodologies", *C. R. Mec.* **345** (2017), no. 12, p. 832-843.

[24] A. Fernandez Del Rincon, F. Viadero, M. Iglesias, P. García, A. De-Juan, R. Sancibrian, "A model for the study of meshing stiffness in spur gear transmissions", *Mech. Mach. Theory* **61** (2013), p. 30-58.

[25] M. T. Khabou, N. Bouchaala, F. Chaari, T. Fakhfakh, M. Haddar, "Study of a spur gear dynamic behavior in transient regime", *Mech. Syst. Signal Process.* **25** (2011), no. 8, p. 3089-3101.

[26] A. Hammami, A. F. Del Rincon, F. V. Rueda, F. Chaari, M. Haddar, "Modal analysis of back-to-back planetary gear: experiments and correlation against lumped-parameter model", *J. Theor. Appl. Mech.* **53** (2015), no. 1, p. 125-138.

[27] J. Lin, R. G. Parker, "Planetary gear parametric instability caused by mesh stiffness variation", *J. Sound Vib.* **249** (2002), no. 1, p. 129-145.